Vector dark matter and LHC constraints, including a 95 GeV light Higgs boson

Seyed Yaser Ayazi[1,*], Mojtaba Hosseini[1,†], Saeid Paktinat Mehdiabadi[2,‡] and Rouzbeh Rouzbehi[1,§]

[1]*Physics Department, Semnan University, P.O. Box 35131-19111, Semnan, Iran*
[2]*Department of Physics, Yazd University, P.O. Box 89195-741, Yazd, Iran*

We study LHC searches for an extension of the Standard Model (SM) by exploiting an additional Abelian $U_D(1)$ gauge symmetry and a complex scalar Higgs portal. As the scalar is charged under this gauge symmetry, a vector dark matter (VDM) candidate can satisfy the observed relic abundance and limits from direct dark matter (DM) searches. The ATLAS and CMS experiments have developed a broad search program for the DM candidates, including associate production of Higgs boson, Z boson, and top quark that couple to DM. In this paper, we perform an extensive analysis to constrain the model by using these experiments at LHC. It can be seen that the LHC results can exclude some parts of the parameter space that are still allowed by relic density and the direct detection searches. Using the LHC results, all scalar Higgs portal masses are excluded for the light VDM. Furthermore, exclusion limits on the parameter space of the model by using the new results of the CMS and ATLAS Collaborations for a new light Higgs boson with mass $\sim$95 GeV are provided.

I. INTRODUCTION

The existence of dark matter (DM) is largely known through a variety of astrophysical and cosmological experiments [1]. Although it is measured to be about 26.4% of the total energy density of the Universe via indirect observations, the true nature of DM particles is still unknown. However, we know that DM must be electrically neutral and does not interact with ordinary baryonic matter.

The main effects caused by DM are gravitational, but the existence of a weakly interacting massive particle (WIMP) is often hypothesised, since it leads to the correct relic density for nonrelativistic matter in the early Universe (WIMP miracle) [2]. In general, the dark sector can interact with the Standard Model (SM) particles through the Higgs portal [3]. We consider a $U(1)$ extension of SM in which a scalar mediated between SM and the dark sector and a vector can play the role of a DM particle. Experiments around the world seek to unravel the nature of DM with different strategies. One of these strategies is to search at particle colliders. Such dark particles could be produced in

particle colliders and detected as the large missing transverse momentum produced in association with the SM particles. To have a realistic model, it must satisfy different available constraints from the DM abundance via standard thermal freeze-out processes, direct detection experiments, and the LHC searches for the DM particles. In this regard, we perform an analysis on the model, focusing on relic density, direct detection, and several searches on associate production of Higgs boson, Z gauge boson, and top quark with the DM particle. In particular, we determine the region of parameter space that can be excluded by the searches at LHC. Some of the LHC analyses have reported the data and background event yields in different signal regions. It enables us to find the limits on the DM signal yields by some statistical methods. By implementing the signal selections in an event generator, one can find the DM signal yields in different points of the parameter space. This yield is compared to the limits extracted from the LHC analyses to decide whether a point is allowed or excluded.

The recent results, reported by the CMS and ATLAS Collaborations, indicate an excess in the $\gamma\gamma$ and $\tau\tau$ final states consistent with a light Higgs boson ($\sim$95 GeV) [4–5]. They provide interesting hints for new physics. Motivated by these results, we perform a study to constrain the model by considering a 95 GeV light Higgs boson.

To explain the model and analysis, the paper is organized as follows. In Sec. II, we introduce the model under consideration. In Secs. III and IV, the allowed parameter space of the model is probed by considering the relic density of DM and direct detection experiments. We present the method and the main results for the LHC

[*]Contact author: syaser.ayazi@semnan.ac.ir
[†]Contact author: mojtaba_hosseini@semnan.ac.ir
[‡]Contact author: spaktinat@yazd.ac.ir
[§]Contact author: rouzbehrouzbehi@semnan.ac.ir

constraints on the model by a list of processes in Sec. V. In Sec. VI, the excluded region in the light of the newly observed 95 GeV light Higgs boson is reported. We also study indirect constraint from the H.E.S.S. experiment on the DM candidate in Sec. VII. Finally, Sec. VIII concludes the paper.

II. THE MODEL

For the reader's convenience, we briefly introduce the main characteristics of the model that is fully developed in Ref. [6]. We extend the SM by a dark sector where the $U_D(1)$ Abelian gauge symmetry is spontaneously broken by the dark Higgs mechanism. We introduce a complex scalar S which has a unit charge under $U_D(1)$ and the $U_D(1)$ gauge field V_μ. These new fields are singlet under the SM gauge group. We also consider an additional Z_2 symmetry, under which the vector field V_μ and the scalar field S transform as follows:

$$V_\mu \rightarrow -V_\mu, \qquad S \rightarrow S^*. \qquad (2.1)$$

Because of the imposed Z_2 symmetry under which only the dark gauge boson V_μ is odd, kinetic mixing between the gauge bosons of the $U_D(1)$ and to $U(1)_Y$ is not possible and two sectors will not mix at any order of perturbation theory; therefore, the field renormalization constants are defined independently in each sector [7–9]. Therefore, the vector field V_μ can be considered as a DM candidate. The total Lagrangian of the model is given by

$$\mathcal{L} = \mathcal{L}_{\mathrm{SM}} - \frac{1}{4}V_{\mu\nu}V^{\mu\nu} + (D'_\mu S)^*(D'^\mu S) - V(H,S), \qquad (2.2)$$

where $\mathcal{L}_{\mathrm{SM}}$ is the SM Lagrangian without the Higgs potential term and the covariant derivative and field strength of V_μ are given as

$$D'_\mu S = (\partial_\mu + ig_v V_\mu)S,$$
$$V_{\mu\nu} = \partial_\mu V_\nu - \partial_\nu V_\mu.$$

The potential, which is renormalizable and invariant under gauge and Z_2 symmetry, is

$$V(H,S) = -\mu_H^2 H^\dagger H - \mu_S^2 S^* S + \lambda_H (H^\dagger H)^2$$
$$+ \lambda_S (S^* S)^2 + \lambda_{SH}(S^* S)(H^\dagger H). \qquad (2.3)$$

The quartic interaction, $\lambda_{SH}(S^*S)(H^\dagger H)$, is the only connection between the dark sector and the SM. The SM Higgs field as well as dark scalar field can receive vacuum expectation values, breaking the electroweak and $U_D(1)$ symmetries, respectively. In this gauge, we write down the Higgs field as

$$H = \frac{1}{\sqrt{2}}\begin{pmatrix} 0 \\ \nu_1 + h_1 \end{pmatrix} \qquad (2.4)$$

and S as

$$S = \nu_2 + h_2. \qquad (2.5)$$

ν_1 and ν_2 are vacuum expectation values of Higgs fields in which we suppose $\nu_1 = 246$ GeV. After the electroweak symmetry breaking [6], the parameters of the model are given by

$$\nu_2 = \frac{M_V}{g_v}, \qquad \sin\alpha = \frac{\nu_1}{\sqrt{\nu_1^2 + \nu_2^2}},$$
$$\lambda_H = \frac{\cos^2\alpha M_{H_1}^2 + \sin^2\alpha M_{H_2}^2}{2\nu_1^2},$$
$$\lambda_S = \frac{\sin^2\alpha M_{H_1}^2 + \cos^2\alpha M_{H_2}^2}{2\nu_2^2},$$
$$\lambda_{SH} = \frac{(M_{H_2}^2 - M_{H_1}^2)\sin\alpha\cos\alpha}{\nu_1\nu_2}, \qquad (2.6)$$

where α is the mixing angle between weak eigenstates and mass eigenstates. The mass eigenstates of Higgs fields can be written as follows:

$$M_{H_2,H_1}^2 = \lambda_H \nu_1^2 + \lambda_S \nu_2^2 \pm \sqrt{(\lambda_H \nu_1^2 - \lambda_S \nu_2^2)^2 + \lambda_{SH}^2 \nu_1^2 \nu_2^2}, \qquad (2.7)$$

where we suppose $M_{H_1} = 125$ GeV. It is remarkable that this construction is rather minimal, in the sense that only three new free parameters are added: coupling g_v and new mass parameters M_{H_2} and M_V.

We also have studied various theoretical and experimental constraints on the parameter space of the model. For theoretical constraints, we must consider constraints such as perturbativity, unitarity, and positivity of the potential. In this regard, we suppose all theoretical conditions that have been discussed in [6]. For experimental constraints, we consider invisible Higgs decay, relic density, and direct detection bounds. The constraints for invisible Higgs decay are completely similar to [6], but for two other constraints, we extend the studied parameter space.

III. RELIC DENSITY

The evolution of the number density of DM particles (n_X) with time is governed by the Boltzmann equation

$$\dot{n}_X + 3Hn_X = -\langle\sigma_{ann}\nu_{\mathrm{rel}}\rangle[n_X^2 - (n_X^{eq})^2], \qquad (3.1)$$

where H is the Hubble parameter and $n_X^{eq} \sim (m_X T)^{3/2} e^{-m_X/T}$ is the particle density before particles get out of equilibrium.
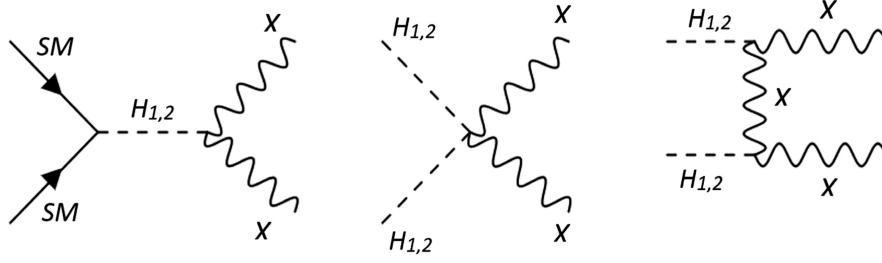
FIG. 1.   The dominant Feynman diagrams for DM relic density production cross section.

The dominant Feynman diagrams for DM production processes are shown in Fig. 1. In this regard, we calculate the relic density numerically for the vector dark matter (VDM) particle by implementing the model into MICROMEGAS [10]. The allowed range of parameter space corresponding to observed DM relic density (according to the data of the Planck Collaboration [11]) is depicted in Fig. 2. As can be seen, there are three mass regions with the correct relic density: (i) $M_V \sim M_{H_2}/2$, (ii) $M_V \lesssim M_{H_2}$, and (iii) $M_V > M_{H_2}$ [9]. In the first case, what is clear is that DM annihilates resonantly via H_2, then the latter decays into SM states (the strip in the figure), and a small mixing angle (α) makes the resonant s-channel annihilation less effective. In the second case, $VV \to H_2 H_2$ annihilation becomes relevant. Of course, when $M_V < M_{H_2}$, due to the thermal tail with high velocity, the correct relic density can be obtained from Ref. [12]. In the third case, DM annihilates into lighter H_2 states. But what is very clear is that the mass window for the resonance and forbidden region (the first and second cases) is quite limited, whereas the case of $M_V > M_{H_2}$ involves much more parameter space. So, the most allowed points of the model are in the region of $60 < M_V < 2000$ GeV and $0.1 < g_v < 1$. Of course, for $M_V < 60$ GeV the $\sin \alpha < 0.44$ constraint is also one of the reasons that limited the parameter space [13,14].
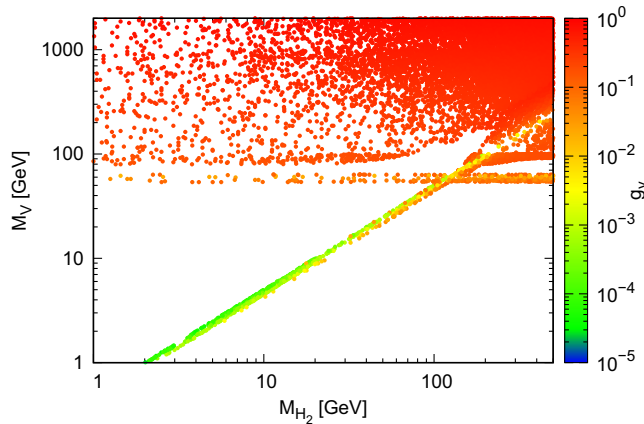
IV. DIRECT DETECTION

Before examining the constraints of LHC on the various channels, let us turn our attention to the direct detection (DD) of VDM in the model. At the tree level, a VDM particle can interact elastically with a nucleon either through H_1 or via H_2 exchange [15]. We use the XENONnT and LUX-ZEPLIN (LZ) experiments results to constrain the parameter space [16,17]. Also for $M_V < 30$ GeV, the results of the XENON1T experiment are used [18]. Figure 3 shows the parameter space of the model in agreement with the DD and relic density constraints. As it can be seen, for different values of the DM mass, there are points that are protected from all the presented phenomenological constraints.

It is necessary to mention that since we are motivated to follow DM phenomenology at the LHC, we consider our parameter space at the electroweak range (1–2000 GeV). In this regard, we used the MICROMEGAS package to calculate the relic density and direct detection constraints. We set 1×10^6 points randomly and obtained those consistent with the allowed relic density and direct detection bound. The final results are shown in Figs. 2 and 3.
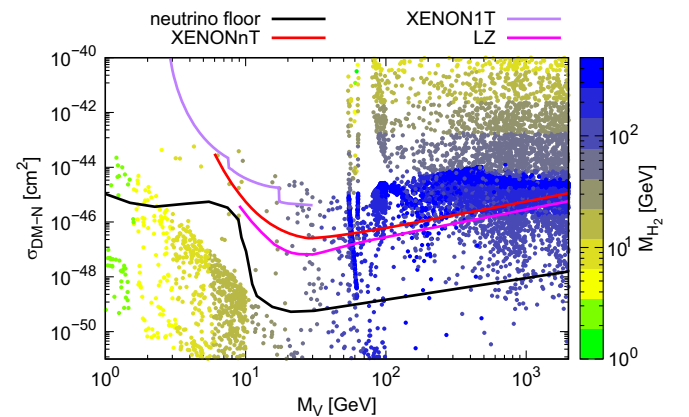

FIG. 2.   The allowed range of parameter space consistent with the DM relic density.

FIG. 3.   The allowed range of parameter space consistent with the DM relic density and DD.

V. THE LHC SEARCHES AND THE DM CONSTRAINTS

The LHC experiments at CERN have done a long list of searches for new physics beyond the SM (BSM) and also measurements of SM cross sections and variables. Up to this date, no sign of new physics or significant deviation from the SM predictions has been reported. This lack of experimental evidence for new physics can be used to constrain any newly introduced extension of SM, e.g., the proposed DM model. To produce the results of this section, the event yields and uncertainties reported by the LHC experiments are used to find the 95% and 68% confidence level (CL) upper limit on the event yields of BSM. The procedure is done using the tools provided in the ROOT [19] analysis framework. It is based on a likelihood ratio semi-Bayesian method [20,21]. The idea is to find the maximum room for events from BSM, by comparing the expected number of events from the SM and the observed event yields in data. The authors have used a similar method to constrain other physics BSM in Ref. [22].

To find the upper limits, 20% total statistical and systematic uncertainty is assumed on DM signals. To make sure the results do not depend on this value, the values of 15% and 25% are also used for this total uncertainty and the changes in the results are found to be marginal. The found maximum number of BSM events is divided by the corresponding integrated luminosity to find the upper limit on the cross section times the acceptance times the experimental efficiency of the BSM in question. To continue, this quantity is called the upper limit of the visible cross section ($\sigma_{\rm vis}^{UL}$). For various channels, $\sigma_{\rm vis}^{UL}$ values are shown in Table I.

To generate the events MADGRAPH5AMC@NLOv.3.4.2 [23] (MG) is used, but to make the model understandable by MG, the introduced model is implemented in LANHEP [24]. The output of this package can be used in MG, easily. The analysis selections are implemented in MG to simulate the experimental acceptance as accurately as possible. The generated events are passed to PYTHIA8 [25] for patron showering and hadronization. The experimental efficiency within the acceptance is assumed to be 100%, which is an optimistic assumption and ends up with conservative results

in the shown plots. To have a more realistic estimation of the efficiencies, one needs to pass the generated events through the full detector simulation and reconstruct the events in detail, which is beyond the scope of this analysis. In most of the LHC analyses, there are several signal regions (bins). The event yields from SM prediction in different bins are summed up and treated as a single bin analysis. The same is done for the collision data, also. Special attention is paid to have completely separated bins and one event has no chance to appear in two different bins and be taken into account two times. For each test point, the input parameters are set in MG and 10000 events are generated to measure the production cross section of that test point. The measured cross section by MG is compared with $\sigma_{\rm vis}^{UL}$. Only a test point with a measured production cross section less than $\sigma_{\rm vis}^{UL}$ is considered as an allowed point; otherwise, it is marked as excluded.

A. LHC constraints on $H + {\rm DM}$

Both multipurpose LHC experiments have reported results on the search for associate production of the Higgs boson and DM. Some of the leading order Feynman diagrams, contributing in this process, are shown in Fig. 4. One of the most interesting decay modes of the Higgs boson is its decay to two photons via a top quark mediated loop. Since the proposed model is implemented in leading order, it cannot handle such decays and this final state is ignored in this analysis. To continue, the decays of the Higgs boson to two τ leptons or two b quarks are considered. The CMS experiment has reported the event yields of the SM prediction and collision data after applying the cuts in events with an SM Higgs boson and the missing transverse momentum in Ref. [26]. The analysis uses 35.9 fb^{-1} of data in $\sqrt{s} = 13$ TeV. The paper contains the results of Higgs boson decay to two b quarks. A special algorithm is used to identify the Higgs bosons with medium Lorentz boost, where b jets produced in the decay of the Higgs boson are merged and appear as a large-radius jet. The yields are reported in four nonoverlapping bins of the missing transverse momentum. The ATLAS experiment has done a similar search using 139 fb^{-1} of data in $\sqrt{s} = 13$ TeV [27]. They also use a variable-radius track-jet algorithm to treat the boosted Higgs
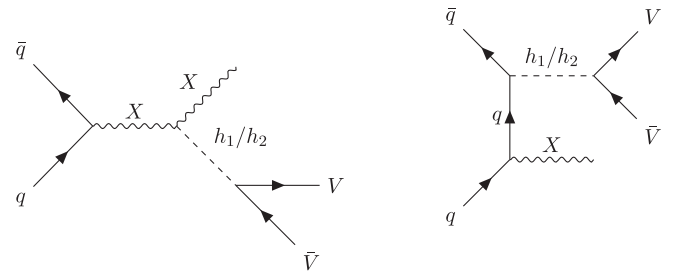
TABLE I. The upper limit of the visible pp cross section ($\sigma_{\rm vis}^{UL}$) for different channels based on the LHC searches at $\sqrt{s} = 13$ TeV.

| | $\sigma_{\rm vis}^{UL}$ (fb) | | | |
| | CMS | | ATLAS | |
Channel	95% CL	68% CL	95% CL	68% CL
$VVZ, Z \to \ell^+\ell^-$	1.22	0.66	4.43	3.41
$H_1VV, H_1 \to \tau^+\tau^-$	0.75	0.39	0.06	0.03
$H_1VV, H_1 \to b\bar{b}$	1.75	0.92	2.6	1.36
$t\bar{t}VV$	85.91	44.1	0.66	0.39

FIG. 4. Feynman diagrams relevant for the production of $X = Z/H_1$ in association with DM at the LHC in the process $pp \to XVV$.

(a) CMS   (b) ATLAS
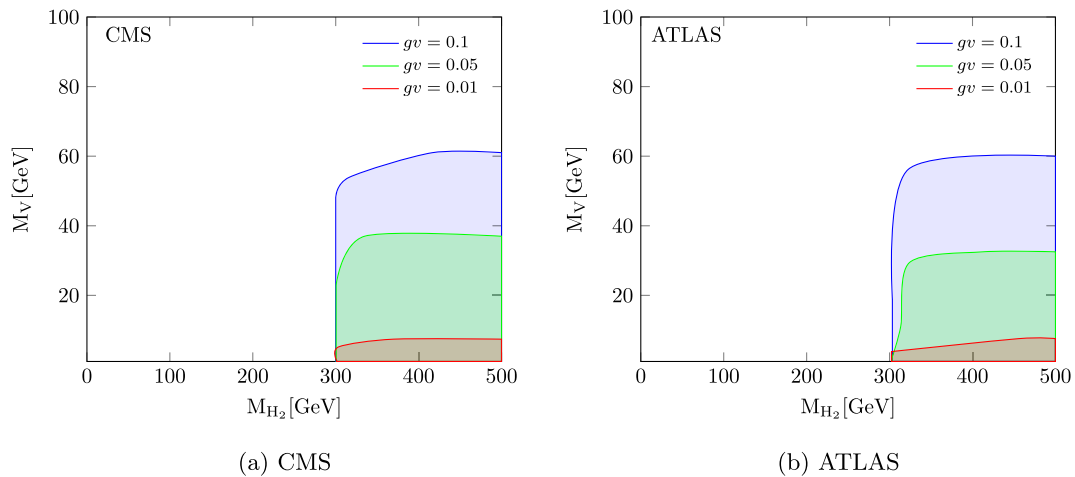
FIG. 5.   The colored regions are excluded at 95% CL by CMS (a) and ATLAS (b) measurements in $pp \to H_1 VV$ ($H_1 \to b\bar{b}$) channel for different g_v values.

bosons properly. For events with exactly two b jets, five exclusive bins of the missing transverse momentum are defined to report the yields.

Figure 5(a) shows the excluded regions in 95% CL in the (M_V, M_{H_2}) plane for different g_v values using the CMS results. A similar result by using the ATLAS measurements is shown in Fig. 5(b).

In Ref. [28], the CMS experiment considers the events consistent with the decay of the Higgs boson to two τ leptons to search for DM produced next to the Higgs boson. The analysis uses 35.9 fb^{-1} of data in $\sqrt{s} = 13$ TeV. Because of different decay modes of the τ lepton, three final states are defined. Events with both τ leptons decay hadronically, or one of them decays hadronically and the other one decays to an electron or a muon, characterize these final states. No further binning is applied. The ATLAS experiment has reported the results of a similar search based on 139 fb^{-1} of data in the same center-of-mass energy in Ref. [29]. Only the

hadronically decaying τ leptons are considered in this paper. The analysis defines two mass ranges. The high mass range is optimized for the booted Higgs bosons, but it is not completely separated from the low mass range. To avoid the complexities due to overlapping signal regions, only the low mass range is used in our analysis. Figure 6(b) shows the excluded regions in 95% CL in the (M_V, M_{H_2}) plane for different g_v values using the CMS results. A similar result by using the ATLAS measurements is shown in Fig. 6(a). The reaches in M_{H_2} direction are comparable, but ATLAS is more powerful in the M_V direction. The ATLAS experiment uses more data, and this can be the source of this superiority.

B. The LHC upper bounds for $pp \to t\bar{t} + \mathrm{DM}$

Associate production of DM and top quark pair ($t\bar{t}$) can happen in Feynman diagrams like Fig. 7. The LHC experiments have reported several analyses on the search
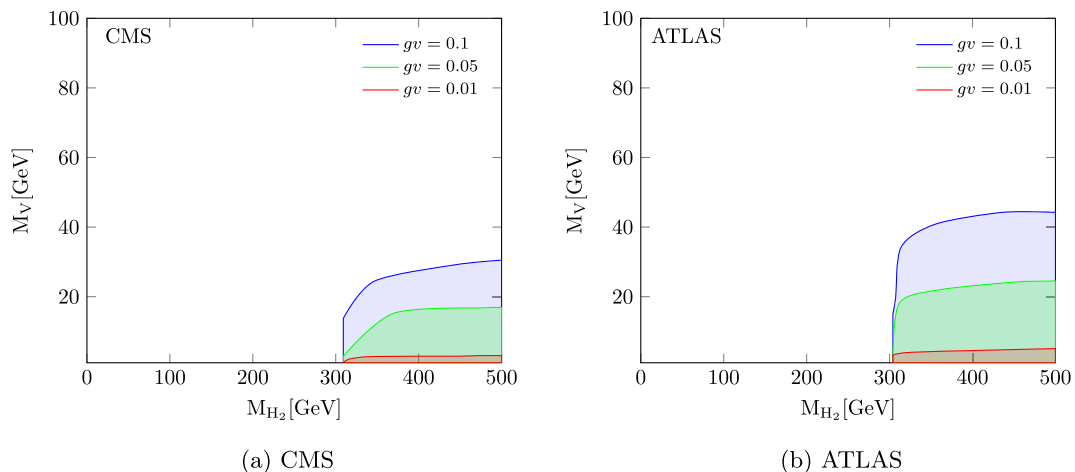

(a) CMS   (b) ATLAS

FIG. 6.   The colored regions are excluded at 95% CL by CMS (a) and ATLAS (b) measurements in $pp \to H_1 VV$ ($H_1 \to \tau^+\tau^-$) channel for different g_v values.
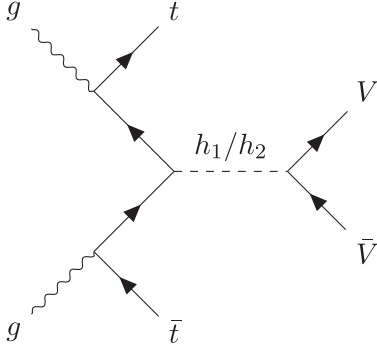
FIG. 7. Feynman diagrams relevant for the production of $t\bar{t}$ in association with DM at the LHC in the process $pp \to t\bar{t}VV$.

for DM production in association with $t\bar{t}$. In this paper, only the latest analyses are considered. The CMS experiment has used 2.2 fb^{-1} of data in $\sqrt{s} = 13$ TeV for this search [30]. The analysis combines the results from different $t\bar{t}$ final states, including zero, one or both top quarks decay hadronically. In all hadronic $t\bar{t}$ events, a special discriminator is used to categorize the events based on the number of the resolved top tagged. It helps to include in the analysis the boosted top quarks which may have some overlaps between the jets. On the other hand, the ATLAS experiment has used 36.1 fb^{-1} of data in the same center-of-mass energy [31]. They have presented the results for three sets of selection criteria when only fully hadronic and fully leptonic decays of $t\bar{t}$ are considered. They also have special treatment for highly boosted top quarks, by using the large-radius jets. Figure 8(b) shows the parts of (M_V, M_{H_2}) parameter space, excluded at 95% CL using CMS results when different g_v values are assumed. The same result by using the ATLAS measurements is shown in Fig. 8(a). Similar to the previous section, ATLAS uses more data and is more powerful in the M_V direction. Comparing to Figs. 5 and 6, this channel is more powerful in the M_{H_2}

direction. Our analysis using this channel can exclude all M_{H_2} values for low M_V, which is a significant achievement.

C. LHC constraints on Z+DM

The Feynman diagrams like Fig. 4 can contribute in associate production of the Z boson and DM. The CMS experiment has reported the event yields of the backgrounds and data after applying the cuts in events with a Z boson and the missing transverse momentum [32]. The analysis uses 137 fb^{-1} of data in $\sqrt{s} = 13$ TeV for the search for DM produced in association with a leptonically decaying Z boson. The results for dielectron and dimuon final states are summed up and reported in two jet multiplicity, zero, and one jet categories. Moreover, the ATLAS experiment has reported results on the same channel by applying different selection cuts [33]. The analysis uses 36.1 fb^{-1} of data in the center-of-mass energy of 13 TeV. The results are reported for dimuon and dielectron final states separately, and no further binning is done. Figure 9(b) shows the parts of (M_V, M_{H_2}) parameter space, excluded at 95% CL using CMS results when different g_v values are assumed. The same result by using the ATLAS measurements is shown in Fig. 9(a). Two experiments have similar reaches in low M_{H_2}, but the CMS experiment, which uses more data in this channel, has a better exclusion for M_V in high M_{H_2}. Comparing with other LHC constraints, this channel gives the best exclusion. It can increase the exclusion in both M_V and M_{H_2} directions comparing to DD results shown in Fig. 3.

VI. LHC CONSTRAINTS ON VECTOR DARK MATTER MODEL WITH A 95 GeV LIGHT HIGGS

Recently, the CMS Collaboration has reported new results, indicating a signal excess with a local (global)
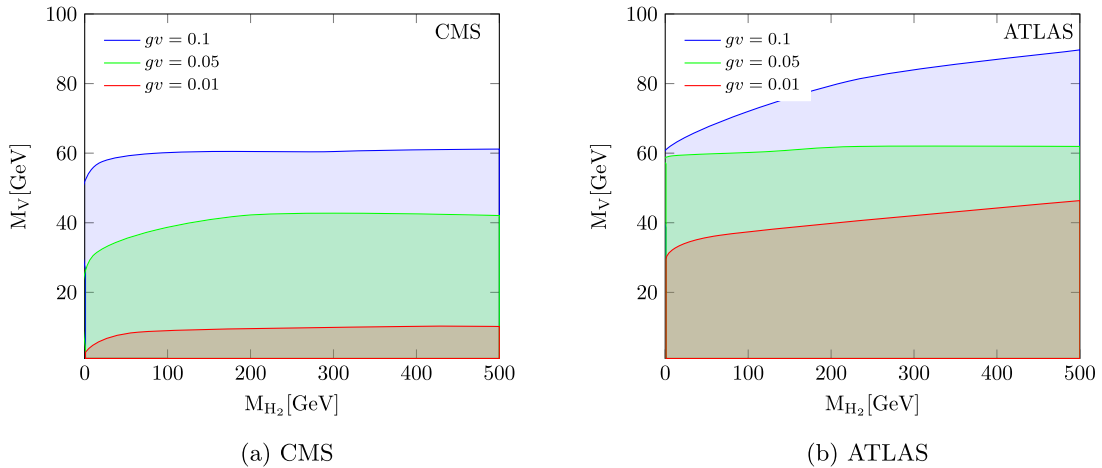

(a) CMS

(b) ATLAS

FIG. 8. The colored regions are excluded at 95% CL by CMS (a) and ATLAS (b) measurements in $pp \to t\bar{t}VV$ channel for different g_v values.

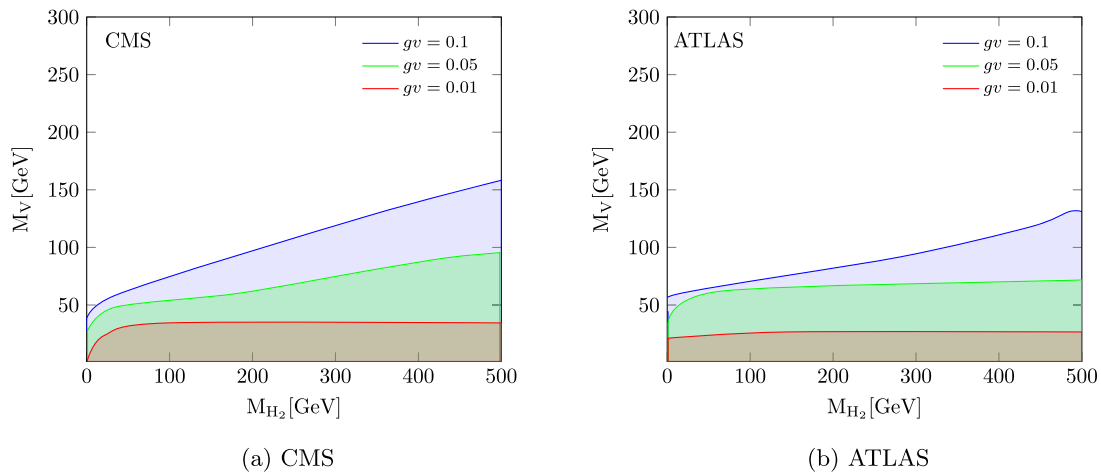(a) CMS   (b) ATLAS

FIG. 9.   The colored regions are excluded at 95% CL by CMS (a) and ATLAS (b) measurements in $pp \rightarrow ZVV$ ($Z \rightarrow \ell^+\ell^-$) channel for different g_v values.

significance of 2.9σ (1.3σ) in the diphoton final state around 95 GeV, using all LHC data collected at $\sqrt{s} = 13$ TeV [4]. The ATLAS group also has reported a similar excess with a local significance of 1.7σ [5]. Further anomalies in the $\tau\tau$ [34] and $b\bar{b}$ [35] final states have been reported by the CMS and LEP Collaborations, respectively. The impact of these reports has been studied in a variety of different BSMs [36–64]. In the proposed model, the new Higgs emerges as a promising candidate. In this regard, H_2 is assumed to be the newly observed particle, and $m_{H_2} = 95$ GeV. Looking at Figs. 5–9 shows only the processes $pp \rightarrow t\bar{t}VV$ and $pp \rightarrow ZVV$ ($Z \rightarrow \ell^+\ell^-$) have sensitivity in m_{H_2} close to 95 GeV. Therefore, the results of these channels are used to constrain the proposed model in the light of the newly observed 95 GeV excess. Figures 10 and 11 show the excluded regions in the $M_V - g_v$ plane, for $pp \rightarrow ZVV$ ($Z \rightarrow \ell^+\ell^-$) and $pp \rightarrow t\bar{t}VV$, respectively. The results based on the analysis of both CMS and ATLAS

Collaborations are shown. Apart from very low values of g_v for both channels and both collaborations, M_V values below 60 GeV are excluded. Dependence on M_V is small, but in low values of g_v, dependence on this parameter is large, and small changes in coupling can switch between allowed and excluded regions. Similar behavior was seen in the previous shapes (Figs. 5–9) also, when the sensitive area is for g_v between 0.01 and 0.1 and beyond this range, no sensitivity is seen.

It is necessary to mention that we consider the model in the leading order and it is impossible to study the decay of H_2 to diphoton. Looking at Fig. 12, it can be seen that H_2 can decay to diphoton when loop corrections are considered. In our study, we only check, if H_2 is responsible for the reported diphoton excess, which part of the parameter space is preferred. Checking the complete consistency between H_2 of the model with the reported excess needs more details from the experiments (data and background

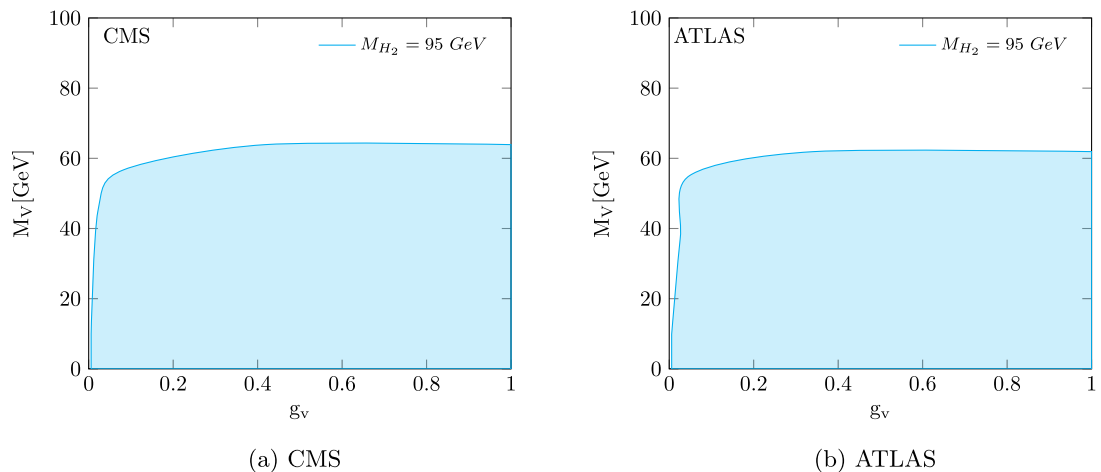(a) CMS   (b) ATLAS

FIG. 10.   The colored regions are excluded at 95% CL by CMS (b) and ATLAS (a) measurements in $pp \rightarrow ZVV$ ($Z \rightarrow \ell^+\ell^-$) channel for different g_v values. The mass of H_2 is fixed to 95 GeV.
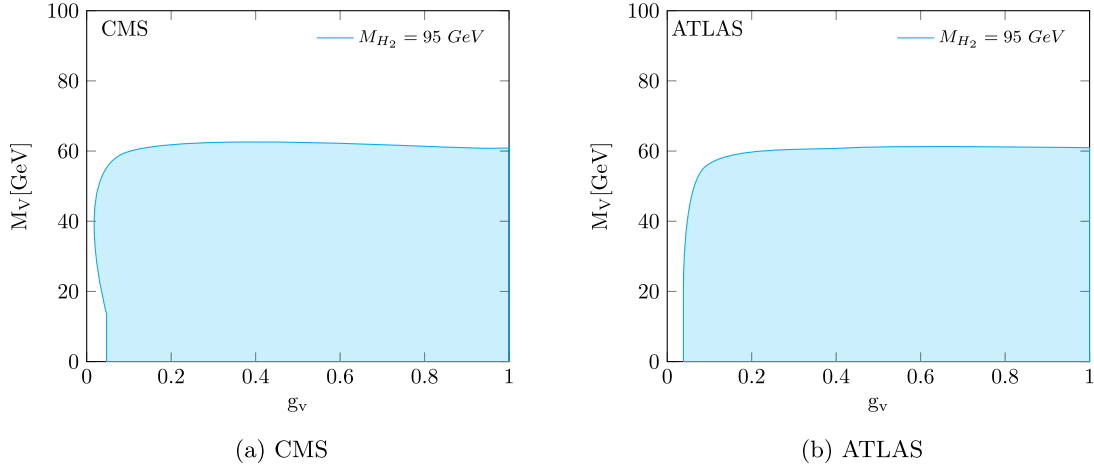
FIG. 11. The colored regions are excluded at 95% CL by CMS (b) and ATLAS (a) measurements in $pp \rightarrow t\bar{t}VV$ channel for different g_v values. The mass of H_2 is fixed to 95 GeV.
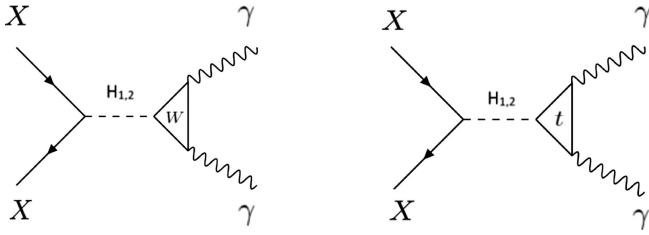

FIG. 12. The dominant Feynman diagrams for the annihilation of a DM pair into monochromatic γ-ray lines.

yields in the vicinity of 95 GeV), which is not provided in the CMS and ATLAS papers or a complete analysis with full detector simulation and reconstruction of signal and backgrounds and comparison with LHC data. The former part is not accessible to the public yet; furthermore, the latter part is beyond the scope of this analysis.

VII. THE H.E.S.S. UPPER BOUND

Indirect detection experiments of DM can be an attractive avenue for signs of DM. Photons, neutrinos, and positrons are the most important products from the annihilation of DM, among which photons are the best option due to their larger cross section and clearer signals. The H.E.S.S. experiment checks the cosmic γ-rays in the photon energy range of 0.03–100 TeV so it can observe high energy processes in the Universe [65]. The monochromatic lines of photons are one of the promising messengers in the indirect search for DM. In our model, DM can annihilate to two photons through quantum loop corrections. The dominant Feynman diagrams contributing to this process are shown in Fig. 12. The cross section is as follows:

$$\sigma(s)v = \frac{1}{4\pi s} |M_{XX \rightarrow \gamma\gamma}|^2, \tag{7.1}$$

where $\sqrt{s}$ is the center-of-mass energy. The amplitude $M_{XX \rightarrow \gamma\gamma}$ is given by

$$M_{XX \rightarrow \gamma\gamma}(s) = ig_v^2 v_2 \left[\frac{i \sin\theta}{s - m_{H_1}^2 - im_{H_1}\Gamma_{H_1}} M_{H_1 \rightarrow \gamma\gamma}(s) \right.$$
$$\left. + \frac{i \cos\theta}{s - m_{H_2}^2 - im_{H_2}\Gamma_{H_2}} M_{H_2 \rightarrow \gamma\gamma}(s) \right], \tag{7.2}$$

where

$$M_{H_1 \rightarrow \gamma\gamma} = \frac{\alpha g_e s \cos\theta}{8\pi M_W} \left[3\left(\frac{2}{3}\right)^2 F_t + F_W \right], \tag{7.3}$$

$$M_{H_2 \rightarrow \gamma\gamma} = \frac{\alpha g_e s \sin\theta}{8\pi M_W} \left[3\left(\frac{2}{3}\right)^2 F_t + F_W \right]. \tag{7.4}$$

Here, $g_e = 2\sqrt{\pi\alpha}/\sin\theta_w$ and

$$F_t = -2\tau[1 + (1 - \tau)f(\tau)], \tag{7.5}$$

$$F_W = 2 + 3\tau + 3\tau(2 - \tau)f(\tau), \tag{7.6}$$

where $\tau = \frac{4m_i^2}{s}$ with $i = t, W$ and

$$f(\tau) = \begin{cases} \left(\sin^{-1}\sqrt{\frac{1}{\tau}}\right)^2 & \text{if } \tau \geq 1 \\ \frac{-1}{4}\left(\ln\frac{1+\sqrt{1-\tau}}{1-\sqrt{1+\tau}} - i\pi\right)^2 & \text{if } \tau < 1. \end{cases} \tag{7.7}$$

Therefore, the annihilation cross section of a pair of DM into two photons is as follows:
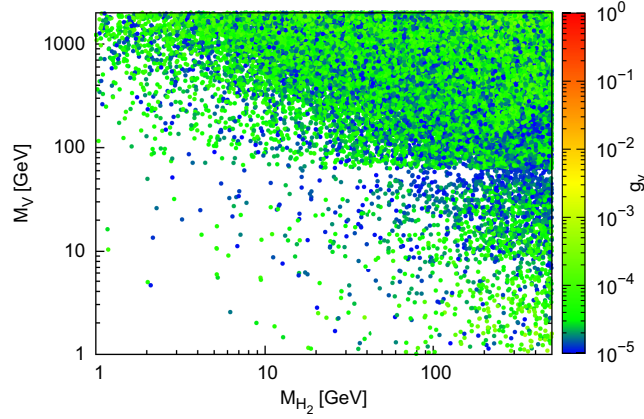
FIG. 13. The allowed range of parameter space consistent with H.E.S.S. data.

$$\sigma(s)\nu = \frac{g_v^4 \nu_2^2}{4\pi s} \left| \frac{\sin\theta M_{H_1 \longrightarrow \gamma\gamma}}{s - m_{H_1}^2 - i m_{H_1}\Gamma_{H_1}} + \frac{\cos\theta M_{H_2 \longrightarrow \gamma\gamma}}{s - m_{H_2}^2 - i m_{H_2}\Gamma_{H_2}} \right|^2.$$

$$(7.8)$$

Finally, the average thermal cross section is equal to

$$\langle \sigma(s)\nu \rangle = \frac{1}{8M_V^4 T K_2^2(\frac{M_X}{T})}$$

$$\times \int_{4M_V^2}^{\infty} ds(s - 4M_V^2)\sqrt{s} K_1\left(\frac{\sqrt{s}}{T}\right)\sigma(s), \qquad (7.9)$$

where K_1 and K_2 are modified Bessel functions and T is the freeze-out temperature. Figure 13 shows the allowed parameter space in agreement with the H.E.S.S. experiment. From the comparison of Figs. 13 and 2, it is clear that only for $1 \le M_V \le 10$ and $2 \le M_{H_2} \le 40$ GeV is the parameter space of our model compatible with the H.E.S.S. results. Comparing this figure with relic density and direct detection results indicates that allowed range of parameters space, which can simultaneously explain relic density, direct detection, and the H.E.S.S. experiment, is fairly small for the g_v coupling constant.

VIII. CONCLUSIONS

In this paper, we revisit an extension of the SM by an extra $U_D(1)$ symmetry. The model consists of an extra scalar as the Higgs portal and a vector gauge field as a DM candidate. It is shown that the model can satisfy the observed cosmological DM abundance via the standard freeze-out mechanism and, at the same time, fulfill the theoretical constraints such as perturbativity, unitarity, and positivity of the potential and also experimental constraints such as invisible Higgs decay and DD bounds. In the following, we focus on associate production of Higgs boson, Z gauge boson, and top quark with the VDM. The results of the LHC experiments on similar final states are used to constrain the parameter space of the model. A statistical method is used to find the maximum room for the events from this DM model in LHC data. It is shown that the results of the associate production of Z gauge boson and DM can exclude some parts of parameters space that are still allowed by relic density and the DD searches. In light of the LHC results, this analysis excludes all M_{H_2} values for the light VDM, which is an unprecedented result. Inspired by the newly observed light Higgs boson close to 95 GeV, the model is tested to determine if its new scalar is the light Higgs boson. The excluded parameter space in light of the LHC constraints and this assumption is also reported. In the end, the constraints from the indirect searches are also examined for completeness.

[1] G. Bertone and D. Hooper, History of dark matter, Rev. Mod. Phys. **90,** 045002 (2018).

[2] J. L. Feng, The WIMP paradigm: Theme and variations, SciPost Phys. Lect. Notes **71,** 1 (2023).

[3] O. Lebedev, The Higgs portal to cosmology, Prog. Part. Nucl. Phys. **120,** 103881 (2021).

[4] CMS Collaboration, Search for a standard model-like Higgs boson in the mass range between 70 and 110 GeV in the diphoton final state in proton-proton collisions at $\sqrt{s} = 13$ TeV, arXiv:2405.18149.

[5] ATLAS Collaboration, Search for diphoton resonances in the 66 to 110 GeV mass range using pp collisions at $\sqrt{s} = 13$ TeV with the ATLAS detector, arXiv:2407.07546.

[6] S. Yaser Ayazi and M. Hosseini, W-boson mass anomaly and vacuum structure in vector dark matter model with a singlet scalar mediator, Int. J. Mod. Phys. A **38,** 2340002 (2023).

[7] S. Glaus, M. Mühlleitner, J. Müller, S. Patel, and R. Santos, Electroweak corrections to dark matter direct detection in a vector dark matter model, J. High Energy Phys. 10 (2019) 152.

[8] K. Hashino, M. Kakizaki, S. Kanemura, P. Ko, and T. Matsui, Gravitational waves from first order electroweak phase transition in models with the U(1)$_X$ gauge symmetry, J. High Energy Phys. 06 (2018) 088.

[9] A. Amiri, B. Díaz Sáez, and K. Ghorbani, (sub)GeV dark matter in the U(1)X Higgs portal model, Phys. Lett. B **844,** 138119 (2023).

[10] D. Barducci, G. Belanger, J. Bernon, F. Boudjema, J. Da Silva, S. Kraml *et al.*, Collider limits on new physics within

MICROMEGAS_4.3, Comput. Phys. Commun. **222,** 327 (2018).

[11] Planck Collaboration, Planck 2018 results. VI. Cosmological parameters, Astron. Astrophys. **641,** A6 (2020).

[12] R. T. D'Agnolo and J. T. Ruderman, Light dark matter from forbidden channels, Phys. Rev. Lett. **115,** 061301 (2015).

[13] A. Farzinnia, H.-J. He, and J. Ren, Natural electroweak symmetry breaking from scale invariant Higgs mechanism, Phys. Lett. B **727,** 141 (2013).

[14] A. Farzinnia and J. Ren, Higgs partner searches and dark matter phenomenology in a classically scale invariant Higgs boson sector, Phys. Rev. D **90,** 015019 (2014).

[15] S. Yaser Ayazi and A. Mohamadnejad, Conformal vector dark matter and strongly first-order electroweak phase transition, J. High Energy Phys. 03 (2019) 181.

[16] XENON Collaboration, First dark matter search with nuclear recoils from the XENONnT experiment, Phys. Rev. Lett. **131,** 041003 (2023).

[17] LZ Collaboration, First dark matter search results from the LUX-ZEPLIN (LZ) experiment, Phys. Rev. Lett. **131,** 041002 (2023).

[18] XENON Collaboration, Light dark matter search with ionization signals in XENON1T, Phys. Rev. Lett. **123,** 251801 (2019).

[19] R. Brun and F. Rademakers, ROOT: An object oriented data analysis framework, Nucl. Instrum. Methods Phys. Res., Sect. A **389,** 81 (1997).

[20] R. D. Cousins and V. L. Highland, Incorporating systematic uncertainties into an upper limit, Nucl. Instrum. Methods Phys. Res., Sect. A **320,** 331 (1992).

[21] J. Conrad, O. Botner, A. Hallgren, and C. Perez de los Heros, Including systematic uncertainties in confidence interval construction for Poisson statistics, Phys. Rev. D **67,** 012002 (2003).

[22] S. Paktinat Mehdiabadi and L. Zamiri, W' pair production in the light of CMS searches, J. Phys. G **45,** 055004 (2018).

[23] J. Alwall, R. Frederix, S. Frixione, V. Hirschi, F. Maltoni, O. Mattelaer *et al.*, The automated computation of tree-level and next-to-leading order differential cross sections, and their matching to parton shower simulations, J. High Energy Phys. 07 (2014) 079.

[24] A. Semenov, LANHEP—A package for automatic generation of Feynman rules from the Lagrangian, version 3.2, Comput. Phys. Commun. **201,** 167 (2016).

[25] C. Bierlich *et al.*, A comprehensive guide to the physics and usage of PYTHIA8.3, SciPost Phys. Codebases **2022,** 8 (2022).

[26] CMS Collaboration, Search for dark matter produced in association with a Higgs boson decaying to a pair of bottom quarks in proton-proton collisions at $\sqrt{s} = 13$ TeV, Eur. Phys. J. C **79,** 280 (2019).

[27] ATLAS Collaboration, Search for dark matter produced in association with a standard model Higgs boson decaying into b-quarks using the full run 2 dataset from the ATLAS detector, J. High Energy Phys. 11 (2021) 209.

[28] CMS Collaboration, Search for dark matter produced in association with a Higgs boson decaying to $\gamma\gamma$ or $\tau^+\tau^-$ at $\sqrt{s} = 13$ TeV, J. High Energy Phys. 09 (2018) 046.

[29] ATLAS Collaboration, Search for dark matter produced in association with a Higgs boson decaying to tau leptons at $\sqrt{s} = 13$ TeV with the ATLAS detector, J. High Energy Phys. 09 (2023) 189.

[30] CMS Collaboration, Search for dark matter produced in association with heavy-flavor quark pairs in proton-proton collisions at $\sqrt{s} = 13$ TeV, Eur. Phys. J. C **77,** 845 (2017).

[31] ATLAS Collaboration, Search for dark matter produced in association with bottom or top quarks in $\sqrt{s} = 13$ TeV pp collisions with the ATLAS detector, Eur. Phys. J. C **78,** 18 (2018).

[32] CMS Collaboration, Search for dark matter produced in association with a leptonically decaying Z boson in proton-proton collisions at $\sqrt{s} = 13$ TeV, Eur. Phys. J. C **81,** 13 (2021).

[33] ATLAS Collaboration, Search for an invisibly decaying Higgs boson or dark matter candidates produced in association with a Z boson in pp collisions at $\sqrt{s} = 13$ TeV with the ATLAS detector, Phys. Lett. B **776,** 318 (2018).

[34] CMS Collaboration, Searches for additional Higgs bosons and for vector leptoquarks in $\tau\tau$ final states in proton-proton collisions at $\sqrt{s} = 13$ TeV, J. High Energy Phys. 07 (2023) 073.

[35] LEP Working Group for Higgs boson searches, ALEPH, DELPHI, L3, OPAL Collaborations, Search for the standard model Higgs boson at LEP, Phys. Lett. B **565,** 61 (2003).

[36] A. Belyaev, R. Benbrik, M. Boukidi, M. Chakraborti, S. Moretti, and S. Semlali, Explanation of the hints for a 95 GeV Higgs boson within a 2-Higgs doublet model, J. High Energy Phys. 05 (2024) 209.

[37] T.-K. Chen, C.-W. Chiang, S. Heinemeyer, and G. Weiglein, 95 GeV Higgs boson in the Georgi-Machacek model, Phys. Rev. D **109,** 075043 (2024).

[38] J. Kalinowski and W. Kotlarski, Constraining Higgs sectors of BSM models—the case of 95 GeV Higgs," in *Proceedings of the Workshop on the Standard Model and Beyond* (2024); arXiv:2404.12233.

[39] U. Ellwanger and C. Hugonie, Nmssm with correct relic density and an additional 95 GeV Higgs boson, Eur. Phys. J. C **84,** 526 (2024).

[40] J. Kalinowski and W. Kotlarski, Interpreting 95 GeV di-photon/$b\bar{b}$ excesses as a lightest Higgs boson of the MRSSM, J. High Energy Phys. 07 (2024) 037.

[41] C.-X. Liu, Y. Zhou, X.-Y. Zheng, J. Ma, T.-F. Feng, and H.-B. Zhang, 95 GeV excess in a CP-violating μ-from-ν SSM, Phys. Rev. D **109,** 056001 (2024).

[42] J. Cao, X. Jia, Y. Yue, H. Zhou, and P. Zhu, 96 GeV diphoton excess in seesaw extensions of the natural NMSSM, Phys. Rev. D **101,** 055008 (2020).

[43] J. Cao, X. Jia, J. Lian, and L. Meng, 95 GeV diphoton and bb^- excesses in the general next-to-minimal supersymmetric standard model, Phys. Rev. D **109,** 075001 (2024).

[44] J. Cao, X. Jia, and J. Lian, Unified interpretation of muon $g - 2$ anomaly, 95 GeV diphoton, and $b\bar{b}$ excesses in the general next-to-minimal supersymmetric standard model, arXiv:2402.15847.

[45] S. Ashanujjaman, S. Banik, G. Coloretti, A. Crivellin, B. Mellado, and A.-T. Mulaudzi, SU(2)L triplet scalar as the origin of the 95 GeV excess?, Phys. Rev. D **108,** L091704 (2023).

[46] D. Borah, S. Mahapatra, P. K. Paul, and N. Sahu, Scotogenic $U(1)L\mu$-$L\tau$ origin of $(g - 2)\mu$, W-mass anomaly and 95 GeV excess, Phys. Rev. D **109,** 055021 (2024).

[47] S. Banik, A. Crivellin, S. Iguro, and T. Kitahara, Asymmetric di-Higgs signals of the next-to-minimal 2HDM with a U(1) symmetry, Phys. Rev. D **108,** 075011 (2023).

[48] S. Bhattacharya, G. Coloretti, A. Crivellin, S.-E. Dahbi, Y. Fang, M. Kumar *et al.*, Growing excesses of new scalars at the electroweak scale, arXiv:2306.17209.

[49] R. Benbrik, M. Boukidi, and S. Moretti, Superposition of *CP*-even and *CP*-odd Higgs resonances: Explaining the 95 GeV excesses within a two-Higgs doublet model, arXiv:2405.02899.

[50] M. A. Diaz, G. Cerro, S. Dasmahapatra, and S. Moretti, Bayesian active search on parameter space: A 95 GeV spin-0 resonance in the $(B-L)$SSM, arXiv:2404.18653.

[51] A. Arhrib, K. H. Phan, V. Q. Tran, and T.-C. Yuan, When standard model Higgs meets its lighter 95 GeV Higgs, arXiv:2405.03127.

[52] Z.-f. Ge, F.-Y. Niu, and J.-L. Yang, The origin of the 95 GeV excess in the flavor-dependent $U(1)_X$ model, Eur. Phys. J. C **84,** 548 (2024).

[53] A. Ahriche, M. L. Bellilet, M. O. Khojali, M. Kumar, and A.-T. Mulaudzi, The scale invariant scotogenic model: CDF-II *W*-boson mass and the 95 GeV excesses, Phys. Rev. D **110,** 015025 (2024).

[54] J. A. Aguilar-Saavedra, H. B. Câmara, F. R. Joaquim, and J. F. Seabra, Confronting the 95 GeV excesses within the U (1)'-extended next-to-minimal 2HDM, Phys. Rev. D **108,** 075020 (2023).

[55] U. Ellwanger, C. Hugonie, S. F. King, and S. Moretti, NMSSM explanation for excesses in the search for neutralinos and charginos and a 95 GeV Higgs boson, arXiv:2404.19338.

[56] K. Wang and J. Zhu, 95 GeV light Higgs in the top-pair-associated diphoton channel at the LHC in the minimal dilaton model, Chin. Phys. C **48,** 073105 (2024).

[57] G. Arcadi, G. Busoni, D. Cabo-Almeida, and N. Krishnan, Is there a (pseudo)scalar at 95 GeV?, arXiv:2311.14486.

[58] D. Azevedo, T. Biekötter, and P. M. Ferreira, 2HDM interpretations of the CMS diphoton excess at 95 GeV, J. High Energy Phys. 11 (2023) 017.

[59] P. Escribano, V. M. Lozano, and A. Vicente, Scotogenic explanation for the 95 GeV excesses, Phys. Rev. D **108,** 115001 (2023).

[60] T. Biekötter, S. Heinemeyer, and G. Weiglein, 95.4 GeV diphoton excess at ATLAS and CMS, Phys. Rev. D **109,** 035005 (2024).

[61] J. Dutta, J. Lahiri, C. Li, G. Moortgat-Pick, S. F. Tabira, and J. A. Ziegler, Dark matter phenomenology in 2HDMS in light of the 95 GeV excess, arXiv:2308.05653.

[62] W. Li, H. Qiao, and J. Zhu, Light Higgs boson in the NMSSM confronted with the CMS di-photon and di-tau excesses, Chin. Phys. C **47,** 123102 (2023).

[63] J. Butterworth, H. Debnath, P. Fileviez Perez, and F. Mitchell, Custodial symmetry breaking and Higgs boson signatures at the LHC, Phys. Rev. D **109,** 095014 (2024).

[64] P. S. B. Dev, R. N. Mohapatra, and Y. Zhang, Explanation of the 95 GeV $\gamma\gamma$ and bb^- excesses in the minimal left-right symmetric model, Phys. Lett. B **849,** 138481 (2024).

[65] H.E.S.S. Collaboration, Search for γ-ray line signals from dark matter annihilations in the inner Galactic halo from 10 years of observations with H.E.S.S., Phys. Rev. Lett. **120,** 201101 (2018).